

Optical and electrical properties of Si nanocrystals embedded in SiC matrix

Rimpy Shukla^{1,3,*}, C. Summonte¹, M. Canino¹, M. Allegranza¹, M. Bellettato¹, A. Desalvo², D. Nobili¹, S. Mirabella², N. Sharma³, M. Jangir³, I. P. Jain³

¹CNR-IMM, via Gobetti 101-40129 Bologna, Italy

²CNR-IMM, via Santa Sofia 64-95123 Catania, Italy

³Centre for Non-Conventional Energy Resources, University of Rajasthan, Jaipur, India

*Corresponding author. Tel: (+39) 51-639-9136; Fax: (+39) 51-639-9216; E-mail: rimshu21@gmail.com

Received: 12 May 2012, Revised: 28 May 2012, Accepted: 03 June 2012

ABSTRACT

Silicon nanocrystals (Si NCs) embedded in a dielectric matrix showing tunable band gap properties have recently emerged as attracting top absorbers in silicon based high efficiency multijunction devices. This paper presents optical and electrical characterization of Si NCs in SiC matrix resulting from annealing at 1100 °C of silicon-rich carbide (SRC)/SiC multilayers produced by Plasma Enhanced Chemical Vapour Deposition (PECVD), varying either the Si content in the SRC or the SiC thickness. Simulation of Reflectance and Transmittance spectra in the UV-Vis revealed that 1) the Si crystallization increases with increasing Si content; 2) a severe shrinkage of the multilayers occurs upon annealing due to the release of hydrogen and to crystallisation; 3) the growth of nanocrystals is affected by atomic environment and diffusivity of involved atoms at the investigated temperature. Temperature dependent conductivity measurements are performed on multilayers and on reference layers. The results show evidence of defect state conduction in the SiC matrix. Copyright © 2012 VBRI Press.

Keywords: Si nanodots; SiC; optical reflectance and transmittance; electrical conductance.



Rimpy Shukla is doing her Ph.D. in Physics under supervision of Prof. I.P. Jain from Centre for Non-Conventional Energy Resources (CNER) University of Rajasthan, Jaipur, India. She is working on Synthesis and Characterization of Silicon-Based Quantum Dot Solar Cells at CNR-IMM, Bologna, Italy. Previously she had done M.Phil. and M.Sc in Physics from the University of Rajasthan, Jaipur and University of Bikaner respectively.

Introduction

The possibility of obtaining band gap modulation in silicon nanodots in dielectric matrix, typically SiO₂, has been proven since long [1]. The reduction of the silicon particle diameter to nanometric size produces the formation of minibands with consequent enlargement of the effective band gap [2]. The nanoparticles are formed by depositing a silicon rich material, and then inducing the precipitation of the excess silicon by thermal treatments. The control of the phenomenon is strictly subordinated to the control of the nanoparticle size, which is normally achieved using the multilayer approach [3-5] in the version of Zacharias [6] that proposes a procedure to separately control the density and size of nanocrystals. The

approach consists of depositing multilayers with alternated stoichiometric and silicon rich composition. In this way, the nanoparticles only form in the silicon rich sublayer (=well layer), and the vertical size is controlled by the thickness of the sublayer itself.

Thanks to their quantum confinement capability, silicon nanocrystals, (nc-Si) are presently considered as a leading-edge material as tunable absorbers in the framework of photovoltaic applications, as in principle they allow to optimize the design of multijunction devices better matched to the solar spectrum [7]. For the embedding dielectric matrix, a trade-off between confining properties and acceptable conductivity is desired. Under this respect, the SiC matrix, among others (typically SiO₂ or Si₃N₄), is considered more promising, because of better conduction properties and lower barrier to Si nanoparticles [8]. However, unlike the case of Si/SiO₂ system, the Si/SiC system is less investigated, mainly because of the less ideal properties, such as phase separation, that is less favoured in the case of Si/SiO₂, because the bond energy difference between Si-Si and Si-C (2.34 eV and 3.21 eV respectively) is less than in SiO₂ case (4.82 eV for the Si-O bond energy [9]).

Electrical reports are preferably focussed on doping of the silicon rich carbide material [10], and of nanocrystals [11-14], sometimes inserted in a heterojunction structure

[15]. Some information exists on the electrical properties of unannealed, hydrogenated microcrystalline SiC [16]. However, little attention has been paid to the undoped Si/SiC system. In fact, in the framework of a photovoltaic thin film device, the low recombination requirements are probably better fulfilled with an intrinsic material, with the needed electric field guaranteed by separate thin p- and n-layers, in analogy to the case of a-Si:H p-i-n solar cells. This stresses the importance of an investigation on transport properties of the intrinsic Si/SiC system.

The study of the electrical behaviour of the Si/SiC system raises different issues with respect to the Si/SiO₂ case. In that case, due to the efficient phase separation and the very good insulating properties of the matrix, carrier transport can safely be ascribed to the silicon nanoparticles subsystem, either the nanodots [14] or the disordered nanodot shell [17, 18]. Rather sharp variation of transport properties was in fact observed as a function of composition, as the silicon concentration reaches a value compatible with percolation through nanoparticles [19], which allows us to draw conclusions on the origin of transport phenomena in that case. In the case of the Si/SiC system, the analysis of the electrical behaviour of the sample is complicated by the not negligible contribution coming from the SiC matrix, which shorts the conduction through possible barriers between the nanoparticles, the situation being temperature dependent.

To this purpose, knowledge of the structural composition of the sample (Si to SiC relative volumes; residual amorphous Si and SiC fractions) is an important basis to the understanding of the electrical properties [20]. A powerful method to monitor the phase separation of the SRC-SiC system is to study their optical properties by extracting refractive index – extinction coefficient (n-k) spectra of the component materials [21] and associate those to suitable computer simulation [22] based on the effective medium approximation (EMA) [23]. A correlation with electrical properties then allows us to improve the understanding of the properties of the material.

In this paper, the multilayer superlattices (SL's) are fabricated by PECVD followed by thermal annealing. The optical properties are determined by Reflection and Transmission spectroscopy (R&T), associated to computer simulation performed by the code Optical [22]. It is shown

that the thermally activated electrical behavior of SL samples is correlated with the microscopic structure as determined by the composition obtained from the effective medium approximation (EMA) [23].

Experimental

Four SRC/SiC SL's were fabricated by PECVD both on quartz and on oxidized c-Si substrate. The varying parameters were the SRC composition and the SiC thickness. These samples were labelled according to the form SLx-t, where x is the Si atomic content in the SRC, ranging between 0.55 and 0.75, and t is the SiC thickness, either 3 or 5 nm. In all cases the SL's were made up of 30 SRC/SiC bilayers starting and ending with a stoichiometric SiC layer. The SRC thickness was kept constant and equal to 3 nm. In order to prevent surface oxidation during annealing a 20 nm thick a-Si:H layer was deposited on the top of each multilayer. SiC and Si test single layers were also produced.

PECVD was carried out on substrates heated at 350 °C, with plasma frequency equal to 13.56 MHz and power 4W/cm², at 0.95 mbar chamber pressure, using SiH₄ (6.0 purity), CH₄ (5.5 purity) and H₂ (6.0 purity) as gas precursors. The different SRC compositions were obtained by varying the SiH₄ flow rate between 1.6 sccm and 11.4 sccm, keeping CH₄ and H₂ flow rates equal to 70 sccm and 10 sccm, respectively. The resulting H₂ dilution of the gas mixtures was between 11% and 12%.

All samples were annealed in a resistance furnace at 1100 °C for 30 minutes in fluent N₂:O₂, 10:1. A 4h pre-annealing at 600 °C was intended to eliminate hydrogen from the material. The annealing was followed by a sequence of etching steps: oxide etching, Si etching and surface cleaning. The SiO₂ resulting from the oxidation of the Si top layer was removed in HF:H₂O, 1:10 for 60-120s (VLSI grade HF, 49%, by KMG). Any residual Si is removed from the top of ML's with a 60s etching at 40 °C in 2% tetra methyl ammonium hydroxide (TMAH, semiconductor grade, purchased from Aldrich) solution. The SL's worked as etch-stop. The final sample thickness values are reported in **Table 1**.

H effusion and SiC crystallization were checked by Fourier transform infrared spectroscopy (FTIR). A Thermo Nicolet 5700 spectrometer was used for spectra acquisition. The computation of absorption spectra was

Table 1. x=Si/(Si+C) ratio in the SRC in the SL's, Si and SiC Nominal Volume Fraction after 1100 °C annealing, computed by considering the shrinkage of the Si and SiC components; optically detected SiC volume fraction (the complement to 100% is Si%), amorphous and crystallized Si fraction and total layer thickness; activation energy and exponential prefactor of the conductance as a function of inverse temperature, determined by lateral electrical measurements.

Sample	Theoretical			Optical measurements			Electrical measurements		
	x	V _{Si}	V _{SiC}	SiC %	a-Si %	μc-Si %	d (nm)	E _a (eV)	σ ₀ (S/cm)
μc-Si-10'	-	100	0	0	0	100	128	0.38-0.49	63
μc-Si 30'	-	100	0	0	0	100	130	0.38	93
SL 75-3	0.75	44	56	55	47	53	134	0.21	0.097
SL 65-3	0.65	31	69	62	58	42	132	0.20	0.083
SL 55-3	0.55	13	87	78	82	18	131	0.17	0.023
SL 65-5	0.65	23	77	70	77	23	159	0.19	0.020
μc-SiC	-	0	100	100	-	-	90	0.17	0.011

done taking into account substrate, roughness, and baseline correction, and normalization for the sample thickness.

The composition of test single layers was determined by 3.5 MeV He Rutherford Backscattering (RBS) analysis, while the carbon ratio $1-x = [C]/([Si]+[C])$ was separately checked by X-ray microanalysis, [24] for details. The hydrogen content was determined using Elastic Recoil Detection Analysis (ERDA).

R&T spectra were measured using an Avantes UV-Vis fiber optics spectrophotometer. All R&T measurements reported in this paper were elaborated by the code OPTICAL [22], which is based on multilayer approach combined with the Bruggemann Effective Medium Approximation, associated to χ^2 minimization of the computed to experimental data.

The lateral conductance as a function of temperature was measured on multilayers deposited on oxidized Si using parallel plane silver contacts spaced 1 mm. A two terminal configuration was used in a vacuum cryostat. The temperature was varied in the range 27-100 °C. The ohmicity of the contacts was checked in the range -30V/+30V. Due to the high resistance of the layers, the contact resistance is assumed to be negligible [25].

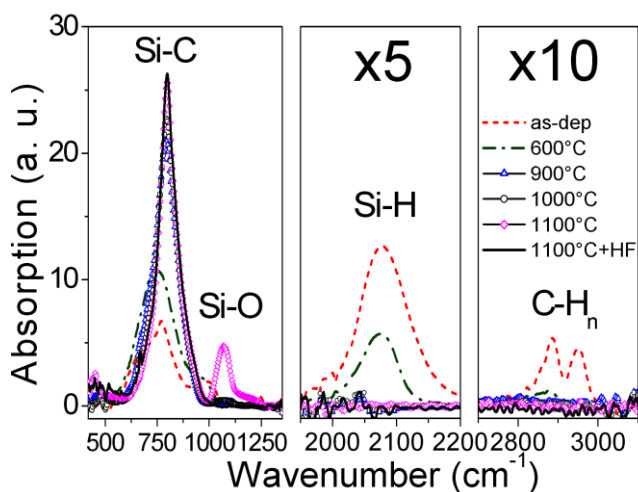


Fig. 1. Fourier transform infrared spectra of SL 75-3, after thickness normalization and baseline subtraction.

Results and discussion

Nanodot formation

The formation of nanodots in this set of samples was evidenced by TEM diffraction and reported [20]. TEM diffraction also shows that the SiC crystallization occurs in the 3C-SiC polytype. Additional information on SiC crystallization comes from FTIR measurements, reported in Fig. 1 after thickness normalization and baseline subtraction. In the figure, the relevant regions of the absorption spectra are shown. The absorption band associated to the Si-C stretching vibration (780 cm^{-1}) increases upon annealing and the shape changes from gaussian to lorentzian, indicating SiC crystallization. The Si-H stretching mode (2050 cm^{-1}) and the C-H_n stretching mode (2900 cm^{-1} , very weak signal) absorption bands

decrease after annealing, indicating the hydrogen release. The 1063 cm^{-1} band (Si-O stretch, after 1100°C treatment) is related to surface oxidation [26].

Sample composition

The composition of reference single-layer samples (Si, SiC, SRC of various compositions) was determined by RBS and ERDA as described in the experimental. Given a SRC of composition $\text{Si}_x\text{C}_{1-x}$, under the hypothesis of complete separation into Si and SiC, the relative volume composition of Si and SiC depends on density and molecular weight. As an example, in an SRC with 50% excess silicon, the silicon volume fraction V_{Si} is as high as 65%, because of the higher density but lower average atomic weight of SiC with respect to Si. A general formula for the Nominal Volume Fraction V_i of a component i for a silicon rich material completely separated into silicon and the silicon alloy(s), such as for instance also silicon rich oxides, silicon rich nitrides, silicon rich oxinitrides, is given by:

$$V_i = \frac{E_i(m_0r_i + m_i)}{\rho_i} \cdot \frac{1}{\sum_i \frac{E_i(m_0r_i + m_i)}{\rho_i}} \quad (1)$$

where $i=0$ refers to silicon and higher numbers refer to the different involved "molecules" (or better, formula units), E_i is the atomic concentration of the element (Si, C, O, or N), ρ_i and m_i are the density and molecular mass of Si, SiC, SiO_2 , and Si_3N_4 , r_0 is zero and r_i (for $i \neq 0$) is the Si-to- E_i ratio in the i -molecule(s) respectively ($=1$ for SiC). In the case of an SRC of composition $\text{Si}_x\text{C}_{1-x}$, then $E_0 = x$ and $E_1 = 1-x$.

The V is important as some quantities are related to the volume occupied by the compound and not to the atomic concentration. For instance, in the optical simulation, the SiC EMA component within the SRC is related to the volume occupied by SiC and not to the concentration of SiC molecules. Also, the total volume occupied by ncSi under complete phase separation is more linked to the V_{Si} than on the Si excess in the sample, which is important in the design of actual devices.

In a SL material composed by SiC barrier layers and SRC well layers with certain silicon Nominal Volume Fraction V_{SiW} as defined in equation (1), the overall V_{Si} is given by:

$$V_{\text{Si}} = V_{\text{SiW}} \cdot \frac{d_w}{d_w + d_B} \quad (2)$$

where d_w and d_B are the thicknesses of the well and the barrier respectively. This quantity is relevant when simulating the SL's using a single EMA superlayer in which the components reflect the overall Si and SiC volume fractions.

Simulation of the R&T spectra

After annealing, the SiC-SRC superlattices undergo the

following processes: hydrogen evolution after the 600°C annealing step, which is needed to prevent cracking of the films upon high temperature annealing; partial or complete crystallization of the SiC matrix; partial or complete separation and crystallization of the Si component [20]. To follow the structural evolution of the samples upon annealing by means of optical simulation, a database is needed for the n-k functions of the component materials. **Fig. 2** reports the n-k functions of the materials involved in the optical simulation. In particular, for amorphous Si we used the n-k files obtained on 600 °C dehydrogenated samples, while for microcrystallized SiC we used the n-k file obtained with from an 1100 °C annealed sample. The n-k files were obtained by fitting the R&T spectra using the Tauc Lorentz approximation as modified by Jellison [27], which was further modified to account for tail absorption (M. Allegranza, unpublished). For microcrystallized Si a literature function was used [28]. The a-SiC component was actually never required in the simulations, and is not reported in the figure. This is in agreement with the crystallization of SiC observed by FTIR.

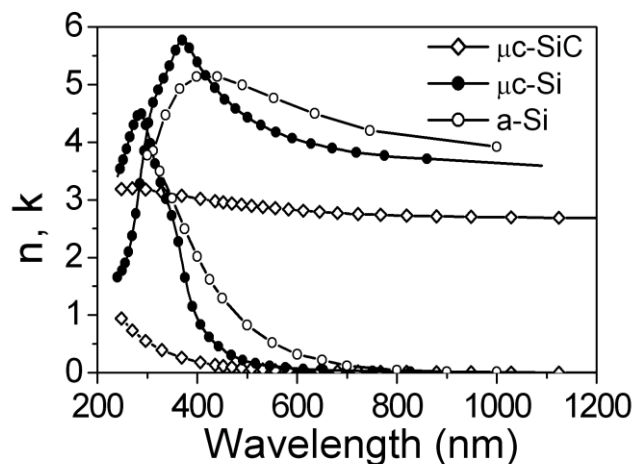


Fig. 2. Spectral n-k for the materials involved in this paper

Such n-k functions were used to simulate the R&T spectra of the as-deposited (not reported) and annealed SL's. The simulations were carried out by using single superlayers described by an EMA composition of microcrystalline SiC and microcrystalline or amorphous Si. The results of the simulation are the amorphous-to-microcrystalline silicon fraction in the EMA, the SiC fraction, and the layer thickness.

Formation of a surface ternary compound

From optical simulation, we systematically observed the formation of a surface layer with low refractive index, which is attributed to the formation of a ternary $\text{Si}_x\text{C}_y\text{O}_z$ compound [29], with composition depending on the underlying material. The hypothesis is supported by FTIR observation, that indicate the appearance of a Si-O related peak after 1100°C annealing (**Fig. 1**). Such surface layer was observed to affect the electrical measurements. For

this reason, we applied a sequence of wet and dry etching to the samples to remove such compound, as briefly described in the experimental. A complete report on the ternary compound and on the procedure needed to remove it will be published soon [26], here we only mention that the electrical measurements reported here are no longer affected by the presence of the surface ternary compound.

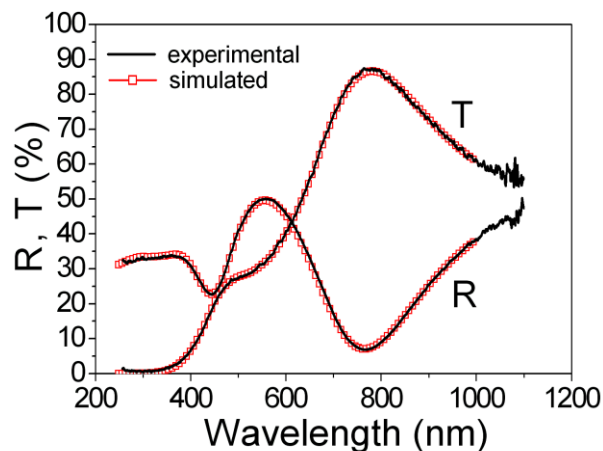


Fig. 3. Experimental and computed R&T spectra of sample SL65-5 after 1100°C annealing.

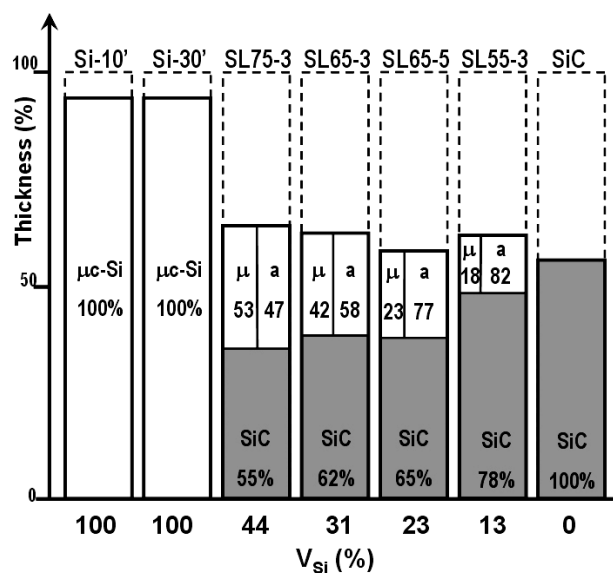


Fig. 4. Sketch illustrating sample thickness variation after annealing, normalized to the as-deposited thickness, and optically determined compositions: SiC fraction, and $\mu\text{C-Si}$ (labelled " μ ") and a-Si (labelled " a ") components of the Si fraction (see **Table 1**).

Results on optical properties

Fig. 3 shows an example of R&T spectra and optical simulation of an 1100°C annealed SL 65-5. The simulation was obtained with a 159 nm thick EMA composed by 65% SiC, and the remaining Si is composed by 77% a-Si and 23% $\mu\text{C-Si}$. The compositional results obtained on all samples are reported in **Table 1**. **Fig. 4** reports the sketches illustrating the obtained results. It is shown that after annealing, severe shrinkage of the samples occurs, depending on the initial sample

composition. We attribute the more marked shrinkage for higher initial carbon concentration to the higher hydrogen incorporation in this case. In fact, for thermodynamical reasons, the probability of existence of Si-H bonds decreases in favour of the formation of C-H bonds as C concentration increases [30]. The occurrence is illustrated in Fig. 5, that reports the variation of thickness of test SiC layers and the hydrogen concentration detected by ERDA as a function of sample composition. The composition dependent shrinkage is to be taken into account in the design of an actual device.

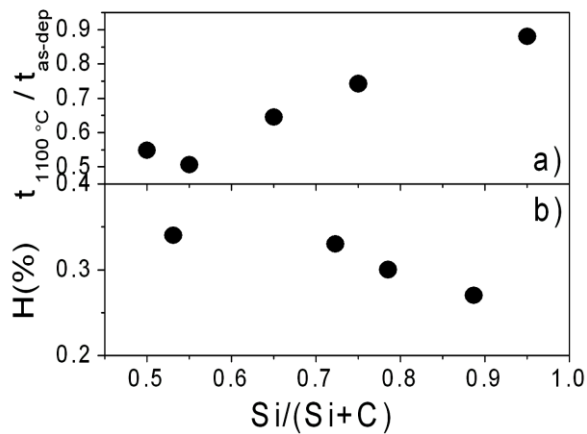


Fig. 5. (a) Thickness variation upon 1100 °C annealing, and (b) H concentration determined by ERDA, for single SRC layers as a function of the Si atomic fraction x .

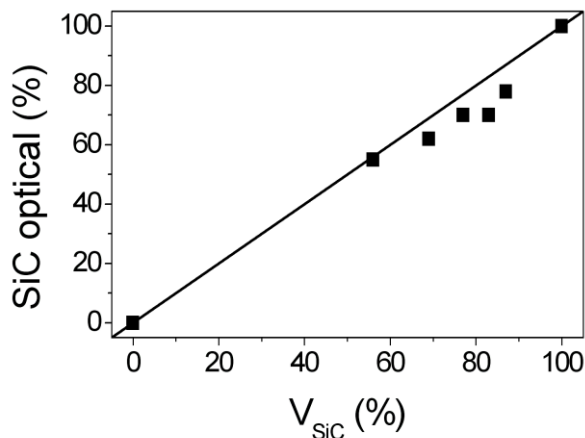


Fig. 6. Optically detected SiC fraction versus nominal volume fraction for 1100°C annealed SL's and reference samples.

To check the validity of optical simulation, in Fig. 6 the optically detected SiC concentration is plotted against the nominal V_{SiC} computed keeping into account the variation of density upon annealing. The observed agreement between the two sets of data confirms the validity of the optically obtained compositional results. The optical results indicate that the $\mu\text{C-Si}$ fraction in the total Si component, namely, $[\mu\text{C-Si}]/([\mu\text{C-Si}]+[\text{a-Si}])$, increases for larger initial V_{Si} (Fig. 4 and Table 1), i.e. the more silicon in the environment, the higher the probability

of crystallization, while small silicon clusters within the SiC matrix tend to remain amorphous. The result is illustrated in Fig. 7 that reports the $\mu\text{C-Si}$ fraction versus the Si atomic concentration in the SRC well layers. In the figure, the thickness of the SiC barrier, as estimated according to the shrinkage observed in single layers, is also indicated. The figure shows that using a thicker SiC barrier layers reduces the crystallized fraction, thus indicating the efficacy of the SiC matrix in limiting the growth of the crystallized domains.

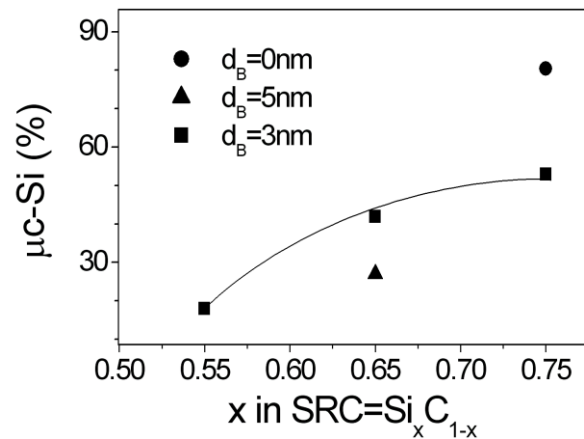


Fig. 7. Optically detected crystallized silicon fraction, as a function of silicon atomic concentration in the well of SL samples. The line connects the data referred to $d_b = 3\text{ nm}$; $d_b = 0\text{ nm}$ indicates a single SRC layer.

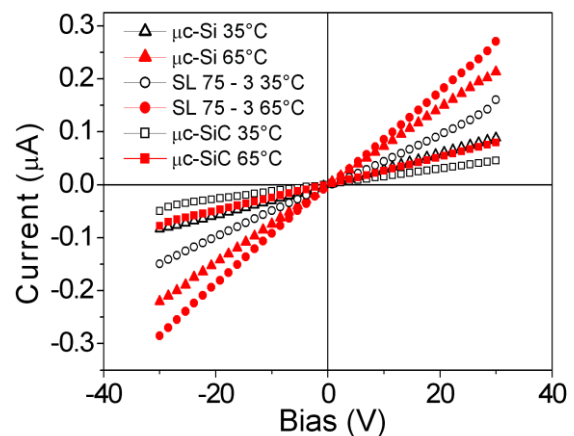


Fig. 8. Room temperature I-V characteristics of SL's and reference samples.

Electrical properties

All samples were measured using a planar configuration and screen printed Ag contacts followed by no annealing. The ohmicity of the contacts was verified through I-V measurements, reported in Fig. 8. The Arrhenius plot of the conductance $\sigma(T)$ of the SL's and of the Si and SiC test single layers is shown in Fig. 9. The figure shows that in all cases the conductivity is thermally activated with a single dependence in the investigated temperature range that can be expressed as:

$$\sigma(T) = \sigma_0 \cdot e^{-E_a/kT}$$

where T is the absolute temperature and k is the Boltzmann constant. The pre-exponential factor and the activation energy E_a are plotted in Figure 10 as a function of the optically detected SiC fraction in the samples, where the values 0 and 100 represent microcrystalline silicon and reference barrier respectively, and all other data refer to SL samples. All data are also reported in **Table 1** for reference. **Fig. 10** shows that both quantities decrease as SiC% increases.

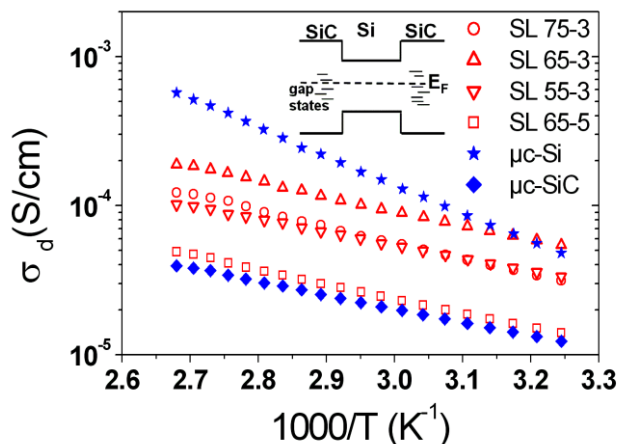


Fig. 9. Conductance as a function of temperature of the SL's and of the two Si and SiC single layers.

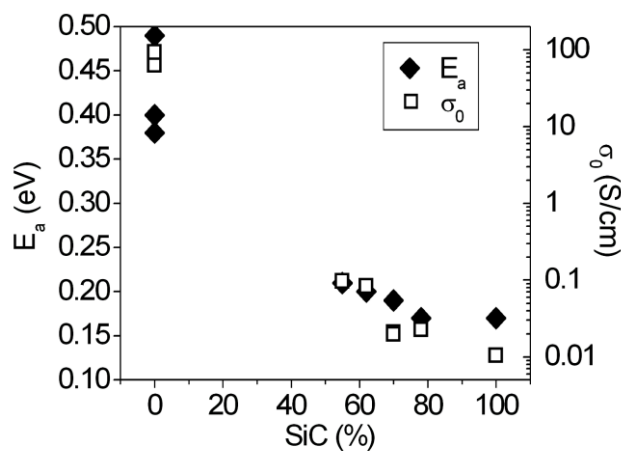


Fig. 10. Activation energy and pre-exponential factor of conductivity Arrhenius plot.

In the case of microcrystallized silicon, (SiC%=0), the high value of the pre-exponential factor and an activation energy in the range 0.37 to 0.5 eV indicates, in our undoped samples, an extended states dominated conduction mechanism, as also confirmed by the existence of photoconductivity (data not reported). For increased SiC fraction concentration, the conductivity pre-exponential factor drops to values in the range 0.01 – 0.1 S/cm while the activation energy decreases to values in the range 0.17

to 0.2 eV. This occurrence, associated to the absence of any photoconductivity signal, indicates that the conduction is dominated by transport through gap states associated to defects, and/or tail states hopping, or percolation through potential fluctuations minima. Given the large band gap of SiC, gap states hopping conduction is compatible with the investigated temperature range. The observed conduction parameters of microcrystallized SiC are also compatible with the presence of an unintended doping impurity, possibly N or O, which was incorporated either during growth or during the successive annealing steps [31]. A similar was indeed already reported for microcrystalline silicon deposited by PECVD [32].

As already observed while discussing **Fig. 4** and **Fig. 7**, the overall silicon crystallized fraction in the SL's is strictly correlated not only with silicon concentration, but also with the thickness of the barrier layer. In fact (see **Fig. 7**), a single layer with $x=0.75$ shows 80% Si crystallized fraction, against the 50% of the same material when inserted in the SL.

The increase of the crystallized fraction with x is related to the dynamics of crystallization that occurs via nucleation and growth of crystalline seeds [33], where nucleation is the limiting step, and decreases for lower silicon volumes [34]. In the case of a SL, the proximity of the interface with SiC lowers the probability of finding Si atoms in the neighborhood, limiting the growth of nanocrystals with respect to the single layer case; the dependence on barrier thickness indicates that diffusivity of the involved atoms at 1100°C is high enough to cause the process to be sensitive not only to Si atoms in close proximity, but to a somewhat wider extent. This is also confirmed by TEM observations which show that, in the case of Si/SiC system, low barrier and well thickness cause the initial multilayer structure to get smeared out upon 1100°C annealing [35]. This result has a dramatic impact on the design of the nc-Si based material in a Si/SiC system where spontaneous phase separation is only moderately favoured. It has the side effect that the nanocrystal size is not only governed by the well layer thickness, but also by the silicon fraction, with the unintended presence of a residual amorphous volume fraction.

In other words, a new parameter, (the residual amorphous Si fraction) beside nanocrystal size and density, arises in the description of the system and needs to be controlled and engineered. The residual amorphous silicon fraction has its impact on electrical and optical properties of the material and must be taken into account in the discussion of the results. Prolonged or more intensive annealing treatments could in principle reduce the residual amorphous fraction; however this solution would not be practical in view of technological applications.

Let's now go back to the discussion of electrical measurements. The activation energy observed for crystallized SiC is compatible with gap states hopping conduction [36]. Hopping conduction is compatible with the large variety of defects that is known to be present

even in epitaxial SiC [37, 38]. One possible defect in our material is the counterpart in 3C-SiC of the EH6/7 in 4H-SiC and 6H-SiC [37, 38], which is located at 0.57 eV below the conduction band and is attributed to a C vacancy.

Basing on optical results, the SL 55-3 only contains an 18% microcrystallized silicon out of the $(1 - \text{SiC}) \% = 22\%$ total silicon fraction (Table 1). The microcrystallized silicon subdomain is therefore below the percolation threshold [19] and we expect the transport being dominated by the surrounding SiC matrix, which is actually the observed result (Fig. 9). Similar considerations apply for SL 65-5. The slightly higher conductivity prefactor (Table 1) probably reflects the lower actual SiC volume (with respect to the 100% used in the determination of σ from I (V) measurements) involved in the conduction mechanism. In SL's with higher silicon concentration, the activation energy and conductivity prefactor increase, indicating increased contribution from the crystallized silicon subdomain, although the resulting room temperature conductivity is actually very similar.

In SL 75-3, we have a 53% silicon crystallized fraction out of the $(1 - \text{SiC}) \% = 45\%$ of the total volume (Table 1), with possibly periodically local higher concentration following the multilayer structure. The conductivity activation energy lower in the case of microcrystallized silicon indicates that a crystallized volume does not form a continuous conduction path within the material. The consequence of the plenty of defects in the SiC matrix and not in the Si nanocrystals has actually the counterintuitive consequence that toward low temperature, the contribution of the SiC matrix dominates, as it is seen at least for the SL 75-3 compared to the $\mu\text{-Si}$ sample in the low T end of the investigated range, see Fig. 9. This occurrence is illustrated in the sketch reported in the inset of Fig. 9. The favoured conduction path then avoids the Si nanoparticles and proceeds through the SiC. In a device in which the SiC is the dielectric matrix producing the confinement of the crystallized Si domains, the existence of gap states causes the carriers generated within the nanodots to tunnel into the SiC matrix, thus preventing the energy collection at the external electrode. For this reason, passivation of the defects is mandatory in view of the application of the material into photovoltaic devices. Indeed, successful experiments of hydrogen plasma passivation of defects in SiC nanocrystals have already been reported [39].

Conclusion

In the present work Reflectance & Transmittance characterization associated to optical simulation is used to determine the evolution of the structure of SiC-SRC superlattices after annealing at 1100°C. The simulation implies the knowledge of the optical constants of the components of the effective medium approximation. By means of optical simulation it has been observed that the crystallized silicon fraction is correlated to the silicon excess in the well sublayer within the superlattices, as well as on the SiC barrier thickness. The results shed light on

the mechanism of formation and growth of the nanocrystals in SiC matrix. For low values of the silicon excess, the conductivity of the material is dominated by the SiC barrier, and is shown to occur via hopping through gap or localized states. Some indication exists on the presence of an unintended dopant impurity that needs to be further investigated. Electrical measurements show that the crystallized silicon subdomain does not form a continuous conduction path, thus confirming the isolated character of nanodots. The importance of passivation required to insert the material in an actual optoelectronic device is emphasised.

Acknowledgements

One of the authors (Rimpy Shukla) undertook this work with the support of the ICTP (International Centre for Theoretical Physics) Programme for Training and Research in Italian Laboratories, Trieste, Italy. The research leading to these results has received funding from the European Community's Seventh Framework Programme (FP7/2007-2013) under grant agreement n°:245977 under the project title NASCEnt.

Reference

- Lu, Z.H.; Lockwood, D.J.; Baribeau, J.M.; *Nature* **1995**, 378, 258. DOI: [10.1038/378258a0](https://doi.org/10.1038/378258a0)
- Yu, P.Y.; Cardona, M.; *Fundamentals of Semiconductors*, Springer Verlag, Berlin, Heidelberg, New York, **1996**.
- Persans, P.D.; Ruppert, A.; Abelès, B.; *Journal of Non-Crystalline Solids* **1988**, 102, 130. DOI: [10.1016/0022-3093\(88\)90123-8](https://doi.org/10.1016/0022-3093(88)90123-8)
- Lockwood, D.J.; Lu, Z.H.; Baribeau, J.M.; *Physical Review Letters* **1996**, 76, 539. DOI: [10.1103/PhysRevLett.76.539](https://doi.org/10.1103/PhysRevLett.76.539)
- Lu, Z.H.; Lockwood, D.J.; Baribeau, J.M.; *Solid-State Electronics* **1996**, 40, 197. DOI: [10.1016/0038-1101\(95\)00245-6](https://doi.org/10.1016/0038-1101(95)00245-6)
- Zacharias, M.; Heitmann, J.; Scholz, R.; Kahler, U.; Schmidt, M.; Bläsing, J.; *Appl. Phys. Lett* **2002**, 80, 661. DOI: [10.1063/1.1433906](https://doi.org/10.1063/1.1433906)
- Wan, Z.; Huang, S.; Green, M.A.; Conibeer, G.; *Nanoscale Res. Lett.* **2011**, 6, 129. DOI: [10.1186/1556-276X-6-129](https://doi.org/10.1186/1556-276X-6-129)
- Jiang, C.W.; Green, M.A.; *J. Appl. Phys.* **2006**, 99, 114902. DOI: [10.1063/1.2203394](https://doi.org/10.1063/1.2203394)
- Smith, F.W.; Yin, Z.; *J. Non-Cryst. Sol.* **1991**, 137, 871. DOI: [10.1016/S0022-3093\(05\)80258-3](https://doi.org/10.1016/S0022-3093(05)80258-3)
- Gradmann, R.; Löper, P.; Künle, M.; Rothfelder, M.; Janz, S.; Hermle, M.; Glunz, S.; *Phys. Status Solidi C* **2011**, 8. DOI: [10.1002/pssc.201000176](https://doi.org/10.1002/pssc.201000176)
- Hao, X.J.; Cho, E.C.; Flynn, C.; Shen, Y.S.; Park, S.C.; Conibeer, G.; Green, M.A.; *Solar Energy Materials & Solar Cells* **2009**, 93, 273. DOI: [10.1016/j.solmat.2008.10.017](https://doi.org/10.1016/j.solmat.2008.10.017)
- Lechner, R.; Stegner, A.R.; Pereira, R.N.; Dietmueller, R.; Brandt, M.S.; Ebbers, A.; Trocha, M.; Wiggers, H.; Stutzmann, J. *Appl. Phys.* **2008**, 104, 053701. DOI: [10.1063/1.2973399](https://doi.org/10.1063/1.2973399)
- Hong, S.H.; Kim, Y.S.; Lee, W.; Kim, Y.H.; Song, J.Y.; Jang, J.S.; Park, J.H.; Choi, S.H.; Kim, K.J.; *Nanotechnology* **2011**, 22, 425203. DOI: [10.1088/0957-4484/22/42/425203](https://doi.org/10.1088/0957-4484/22/42/425203)
- Cavalcoli, D.; Detto, F.; Rossi, M.; Tomasi, A.; Cavallini, A.; *Nanotechnology* **2010**, 21, 045702. DOI: [10.1088/0957-4484/21/4/045702](https://doi.org/10.1088/0957-4484/21/4/045702)
- Song, D.Y.; Cho, E.C.; Conibeer, G.; Flynn, C.; Huang, Y.D.; Green, M.A.; *Solar Energy Materials & Solar Cells* **2008**, 92, 474. DOI: [10.1016/j.solmat.2007.11.002](https://doi.org/10.1016/j.solmat.2007.11.002)
- Yoshida, N.; Terazawa, S.; Takeuchi, A.; Yoneyama, N.; Morino, T.; Jun, Z.; Natsuhara, H.; Nonomura S.; *Phys. Status Solidi C* **2010**, 7, 790. DOI: [10.1002/pssc.200982732](https://doi.org/10.1002/pssc.200982732)
- Balberg, I.; Dover, Y.; Naides, R.; Conde, J.P.; Chu, V.; *Phys. Rev. B* **2004**, 69, 035203. DOI: [10.1103/PhysRevB.69.035203](https://doi.org/10.1103/PhysRevB.69.035203)
- Azulay, D.; Millo, O.; Savir, E.; Conde, J. P.; Balberg, I.; *Phys. Rev. B* **2009**, 80, 245312.

- DOI: [10.1103/PhysRevB.80.245312](https://doi.org/10.1103/PhysRevB.80.245312)
19. Balberg, I.; *J. Appl. Phys.* **2011**, *110*, 061301.
DOI: [10.1063/1.3637636](https://doi.org/10.1063/1.3637636)
 20. Summonte, C.; Canino, M.; Allegranza, M.; Bellettato, M.; Desalvo, A.; Mirabella, S.; Terrasi, A.; *26th EPVSEC*, 5-9 Sept **2011**, Hamburg (D), 361.
 21. Summonte, C.; Centurioni, E.; Canino, M.; Allegranza, M.; Desalvo, A.; Terrasi, A.; Mirabella, S.; Di Marco, S.; Di Stefano, M.A.; Miritello, M.; Lo Savio, R.; Simone, F.; Agosta, R.; *Phys. Status Solidi C* **2011**, *8*, 996–1001.
DOI: [10.1002/pssc.201000413](https://doi.org/10.1002/pssc.201000413)
 22. Centurioni, E.; *Appl. Opt.* **2005**, *44*, 7532.
DOI: [10.1364/AO.44.007532](https://doi.org/10.1364/AO.44.007532)
 23. Bruggeman, D.A.G.; *Ann. Phys.* **1935**, *24*, 636.
 24. Summonte, C.; Rizzoli, R.; Bianconi, M.; Desalvo, A.; Iencinella, D.; Giorgis, F.; *J. Appl. Phys.* **2004**, *96*, 3987.
DOI: [10.1063/1.1786679](https://doi.org/10.1063/1.1786679)
 25. Song, C.; Rui, Y.; Wang, Q.; Xu, J.; Li, W.; Chen, K.; Zuo, Y.; Wang, C.; *J. of Alloys and compounds* **2001**, *509*, 3963.
DOI: [10.1016/j.jallcom.2010.12.191](https://doi.org/10.1016/j.jallcom.2010.12.191)
 26. Canino, M.; Summonte, C.; Allegranza, M.; Shukla, R.; Bellettato, M.; Desalvo, A.; Mancarella, F.; Sanmartin, M.; Terrasi, A.; Löper, P.; Schnabel, M.; Janz, S.; E-MRS 2012 Spring Meeting, Symp. Y, Strasbourg, **2012**. Submitted to *Material Science and Engineering B*.
 27. Jellison, J.G.E.; Modine, F.A.; *Appl. Phys. Lett.* **1996**, *69*, 371.
DOI: [10.1063/1.118064](https://doi.org/10.1063/1.118064)
 28. Jellison, G.E.; Chisholm, M.F.; Gorbalkin, S.M.; *Appl. Phys. Lett.* **1993**, *62*, 3348.
DOI: [10.1063/1.109067](https://doi.org/10.1063/1.109067)
 29. Hornetz, B.; Michel, H.J.; Halbritter, J.; *J. Mat. Res.* **1994**, *9*, 3088.
DOI: [10.1557/JMR.1994.3088](https://doi.org/10.1557/JMR.1994.3088)
 30. Desalvo, A.; Giorgis, F.; Pirri, C.F.; Tresso, E.; Rava, P.; Galloni, R.; Rizzoli, R.; Summonte, C.; *J. Appl. Phys.* **1997**, *81*, 7973.
DOI: [10.1063/1.365400](https://doi.org/10.1063/1.365400)
 31. Summonte, C.; Canino, M.; Allegranza, M.; Bellettato, M.; Desalvo, A.; Shukla, R.; Crupi, I.; Milita, S.; E-MRS 2012 Spring Meeting, Symp. Y, Strasbourg, **2012**.
 32. Torres, P.; Meier, J.; Flückiger, R.; Kroll, U.; Selvan, J.A.A.; Keppner, H.; Shah, A.; *Appl. Phys. Lett.* **1996**, *69*, 1373.
DOI: [10.1063/1.117440](https://doi.org/10.1063/1.117440)
 33. Olson, G.L.; Roth, J.A.; *Material Science Reports* **1988**, *3*, 1.
DOI: [10.1016/S0920-2307\(88\)80005-7](https://doi.org/10.1016/S0920-2307(88)80005-7)
 34. Mirabella, S.; Agosta, R.; Franzò, G.; Crupi, I.; Miritello, M.; Lo Savio, R.; Di Stefano, M.A.; Di Marco, S.; Simone, F.; Terrasi, A.; *J. Appl. Phys.* **2009**, *106*, 103505.
DOI: [10.1063/1.3259430](https://doi.org/10.1063/1.3259430)
 35. López-Vidrier, J.; Hernández, S.; Samà, J.; Canino, M.; Allegranza, M.; Bellettato, M.; Shukla, R.; Schnabel, M.; Löper, P.; López-Conesa, L.; Estradé, S.; Peiró, F.; Janz, S.; Garrido, B.; E-MRS 2012 Spring Meeting, Symp. Y, Strasbourg, **2012**. Submitted to *Material Science and Engineering B*.
 36. Street, R.A.; *Hydrogenated Amorphous Silicon*, Cambridge University Press, U.K., **1991**, pp. 264.
 37. Alfieri, G.; Kimoto, T.; *Mat Sci Forum* **2009**, *615-617*, 389.
DOI: [10.4028/www.scientific.net/MSF.615-617.389](https://doi.org/10.4028/www.scientific.net/MSF.615-617.389)
 38. Beyer, F.; Hemmingsson, C.; Gällström, A.; Leone, S.; Pedersen, H.; Henry, A.; Janzén, E.; *Appl. Phys. Lett.* **2011**, *98*, 152104.
DOI: [10.1063/1.3579527](https://doi.org/10.1063/1.3579527)
 39. Künle, M.; Kaltenbach, T.; Löper, P.; Hartel, A.; Janz, S.; Eibl, O.; Nickel, K.G.; *Thin Solid Films* **2010**, *519*, 151.
DOI: [10.1016/j.tsf.2010.07.085](https://doi.org/10.1016/j.tsf.2010.07.085)

Advanced Materials Letters

Publish your article in this journal

ADVANCED MATERIALS Letters is an international journal published quarterly. The journal is intended to provide top-quality peer-reviewed research papers in the fascinating field of materials science particularly in the area of structure, synthesis and processing, characterization, advanced-state properties, and applications of materials. All articles are indexed on various databases including [DOAJ](http://www.doaj.org) and are available for download for free. The manuscript management system is completely electronic and has fast and fair peer-review process. The journal includes review articles, research articles, notes, letter to editor and short communications.

